Spin-orbit-induced gap modification in buckled honeycomb XBi and XBi3 (X = B, Al, Ga, and In) sheets

Rafael R. Q. Freitas, F. de Brito Mota, R. Rivelino, C. M. C. de Castilho, Anelia Kakanakova-Georgieva, Gueorgui Kosto and Gueorguiev

Original Publication:

Rafael R. Q. Freitas, F. de Brito Mota, R. Rivelino, C. M. C. de Castilho, Anelia Kakanakova-Georgieva, Gueorgui Kosto and Gueorguiev, Spin-orbit-induced gap modification in buckled honeycomb XBi and XBi3 (X = B, Al, Ga, and In) sheets, 2015, Journal of Physics: Condensed Matter, (27), 48, 485306.
http://dx.doi.org/10.1088/0953-8984/27/48/485306

Spin-Orbit-Induced Gap Modification in Buckled Honeycomb XBi and XBi_3 (X = B, Al, Ga, and In) Sheets

R. R. Q. Freitas[1,2], F. de Brito Mota[1], R. Rivelino[1], C. M. C. de Castilho[*,1,3], A. Kakanakova-Georgieva[2] and G. K. Gueorguiev[*,2]

[1]*Grupo de Física de Superfícies e Materiais, Instituto de Física, Universidade Federal da Bahia, Campus Universitário da Federação, 40170-115 Salvador, Bahia, Brazil;*

[2]*Department of Physics, Chemistry and Biology (IFM), Linköping University, 581 83 Linköping, Sweden;*

[3]*Instituto Nacional de Ciência e Tecnologia em Energia e Ambiente (CIENAM) INCT-E&A, Universidade Federal da Bahia, Salvador, Bahia, Brazil*

[*]Corresponding authors: G. K. Gueorguiev (Email: gekos@ifm.liu.se) and C. M. C. de Castilho (Email: caio@ufba.br)

Abstract

The band structure and stability of XBi and XBi_3 (X = B, Al, Ga, and In) single sheets are predicted using first-principles calculations. It is demonstrated that the band gap values of these new classes of two-dimensional (2D) materials depend on both the spin-orbit coupling (SOC) and type of group-III elements in these hetero-sheets. Thus, topological properties can be achieved, allowing for viable applications based on coherent spin transport at room temperature. The spin-orbit effects are proved to be essential to explain the tunability by group-III atoms. A clear effect of including SOC in the calculations is lifting the spin degeneracy of the bands at the Γ of the Brillouin zone. The nature of the band gaps, direct or indirect, is also tuned by SOC, and by the appropriate X element involved. It is observed that, in the case of XBi single sheets, band inversions naturally occur for GaBi and InBi, which exhibit band gap values around 172 meV. This indicates that these 2D materials are potential candidates for topological insulators. On the contrary, a similar type of band inversion, as obtained for the XBi, was not observed in the XBi_3 band structure. In general, the calculations, taking into account SOC, reveal that some of these buckled sheets exhibit sizable gaps, making them suitable for applications in room-temperature spintronic devices.

KEYWORDS: Bismuth, 2D materials, Topological Insulators, DFT, Spin-orbit coupling

1. INTRODUCTION

Intense research in two-dimensional (2D) semiconductor materials has been conducted as prospective graphene alternatives [1-5]. It expands into the group-III nitrides involving the most recognizable example at present, the 2D hexagonal BN [6-8], but also hexagonal AlN [9-12], and hexagonal GaN [13]. More recently elemental phosphorus has been demonstrated to be stable in different structures [14,15]. It is to be noted that group-III nitrides are valuable semiconductor materials in their wurtzite crystal structure. These materials have been successfully developed by the use of metal organic chemical vapor deposition (MOCVD) for implementation in widely spread energy-saving white light-emitting sources [16].

In the same category of III-V materials, the group-III bismuthides are largely unexplored systems. Indeed, there is a lack of experimental data concerning binary compounds such as AlBi, GaBi, and InBi. The properties of these materials have been predicted by density functional theory (DFT) calculations of their band and crystalline structure [17]. More recently, the properties of BBi, AlBi, GaBi, InBi, and TlBi, have been also investigated within DFT [18-19]. Only recently thin films of crystalline InBi have been obtained by molecular beam epitaxy [20]. On the other hand, the overall bismuth chemistry (characterized by its low toxicity) and metallurgy is relatively well known, mainly as a result of Bi application as lead replacement in brass alloys [21] and due to the Bi-alloys low-melting points for special solders [22]. Well known in bearings technology is the Al-Bi metallic alloy system [23]. Some Al-Bi-M (M = Cu, Si, Sn) ternary alloys [24] have also been reported.

An essential factor favoring the research exploration into Bi-containing materials is the availability of Bi-precursors for various deposition techniques, including MOCVD, as employed for depositing bismuth selenides [25], and atomic layer deposition (ALD), as employed for depositing bismuth titanate thin films [26]. While bismuth selenides and tellurides are semiconductors and thermoelectric materials, bismuth titanate, vanadate and other oxides belong to a class of layered perovskite materials, with applications as ferroelectric compounds in electronics and optics [26]. Exfoliated flakes of Bi_2Se_3, Bi_2Te_3 and Bi_4Br_4 are presently associated with the search of quantum spin Hall insulators [27, 28]. It can be envisaged that, due to its finest control of thickness, attempts for the synthesis of 2D hexagonal equivalents of group-III bismuthides may involve ALD. Accordingly, the selection of proper substrates, those with weak interactions, for example

MoS_2, h-BN, as well as hydrogenated surfaces, and also hydrogenated SiC, Si or graphene, are the most promising [29, 30 PRB88 165301].

The 2D hexagonal equivalents of group-III bismuthides are currently an emerging topic [29] in the field of low dimensional materials. First-principles electronic structure calculations predict them to be topological insulators with large enough band gap (~ 560 meV) for room temperature applications. In this work, we comparatively investigate two classes of hexagonal group-III bismuthides with stoichiometry of XBi and XBi_3 (X = B, Al, Ga and In). The latter was inspired by recent DFT calculations, emphasizing the interest in the stability and synthesizability of novel 2D hexagonal sheets with a composition XY_3 (X = B, C, N, Al, P and Y = Si, C) [31-33]. The equilibrium structure of such sheets can be buckled, as in the cases of NSi_3 and PSi_3, while other XSi_3 (X = B, C, Al) are flat [31]. The versatility of XY_3 structures (from buckled at different degrees to completely flat) is complemented by the diversity of their electronic properties. For example, similarly to graphene and silicene, the CSi_3 sheet is predicted to be a zero-band gap semi-metal, while other 2D sheets, such as $AlSi_3$ and PSi_3, are narrow-band gap semiconductors [31]. These findings make such sheets attractive materials for the emerging 2D materials for nanoelectronics.

By employing DFT calculations, we assess the stoichiometric and geometrical compatibility for the equilibrium structures of hexagonal XBi and XBi_3 sheets. The dynamical stability was evaluated by calculating the phonons spectra as well as the energetic stability for all the studied systems. We also focus on the electronic properties of XBi and XBi_3 exploring the spin-orbit effects on their band structure. This paper is structured as follows: after a description of the calculation methods in Section 2, the results and discussions for XBi and XBi_3 2D sheets are presented in Section 3, while the summary and conclusions represent the content of Section 4.

2. COMPUTATIONAL DETAILS

The approaches adopted for all calculations relevant to this work are based on DFT, within its generalized gradient approximation (GGA), as implemented in the VASP code [34]. We employ the Perdew-Burke-Ernzerhof [35] approximation in order to describe the exchange-correlation potentials with the projector augmented wave (PAW) method [36] to describe the electron-ion interaction. This functional has successfully been used to predict the band structures of related Bi-containing layers induced by spin-orbit coupling (SOC) [29, 37]. As Bi is a heavy atom, the SOC is explicitly taken into account

in the band structure calculations, by performing fully non-collinear magnetic structure calculations [38] after obtaining the nonmagnetic ground state of the systems.

The hexagonal sheets of XBi and XBi_3 (X = B, Al, Ga and In) were modelled by employing an hexagonal unit cell containing two and eight atoms, respectively, while the length of the **c** vector was set to 20 Å, so that successive monolayers do not interact along the direction of the **c** vector. The energy cut-off was set to 700 eV and the adopted k-mesh was 25×25×1, and 16×16×1 for the XBi and XBi_3, respectively. For the structural relaxations of the geometric configurations considered, their constituent atoms were allowed to relax until the forces acting on each atom decrease below the value of 0.01 eV/Å. The total energy convergence criterion, in both cases, was set to be 10^{-5} eV. As a complement necessary for assessing the dynamic stability of relaxed XBi and XBi_3 sheets, their phonon spectra were obtained by employing the Density Functional Perturbation Theory (DFPT) method as implemented in the VASP combined with the Phonopy code [39].

Within the adopted scheme, the cohesive energies associated to these 2D systems were also calculated. Cohesive energy per atom ($E_{coh/at}$) is defined as follows:

$$E_{coh/at} = -\frac{1}{N}(E_{AB} - n_A E_A - n_B E_B) \quad (1)$$

In eq. 1, E_A and E_B are the total energies of the free atoms, E_{AB} is the total energy per unit cell of the compound AB, with n_A and n_B being the corresponding numbers of atoms of each element A and B per unit cell and *N* is the total number of atoms. In the case of hexagonal sheets of XBi, $n_A = n_B = 1$, while in the case of hexagonal sheets of XBi_3, $n_B = 3n_A$.

3. RESULTS AND DISCUSSION

3.1. Structure and dynamic stability of the XBi and XBi_3 sheets

We have obtained, after full relaxation, two equilibrium geometries with a distinct buckling parameter, Δ, graphically defined in figure 1(a), as and displayed in figure 1(b), in accordance with ref. [29]. First, we discuss the structural properties of the hexagonal sheets of XBi (X = B, Al, Ga, and In), as shown in figure 1(a). We have obtained, after full relaxation, two equilibrium geometries with a distinct Δ, in accordance with ref. [29]. With the exception of BBi, all the other structures can be classified as low buckled (LB) or high buckled (HB) [40], with, in our systems, the HBs being slightly more favorable than the LB ones. Additionally, we have calculated the phonon spectra of all the XBi

sheets. Only the LB systems are dynamically stable as shown in figure 1(c) for GaBi, which is, in some extent, rather similar to the phonon spectra of buckled blue phosphorus [15]. On the contrary, the HB structures present imaginary frequencies, as shown in figure 1(d) also for the GaBi. In this context, our results indicate that all four hexagonal sheets of BBi, AlBi, GaBi, and InBi represent LB systems.

The structural parameters of the LB equilibrium structures of all XBi sheets are listed in Table 1 with their lattice parameters varying in the range of 3.89 – 4.80 Å. In terms of both lattice constants and buckling parameters, our results are in excellent agreement with those obtained for the same systems, at a similar level of theory [29]. Also in Table 1, for comparative purposes and to put the XBi sheets in an appropriate context, the structural parameters of graphene, silicene and h-BN, calculated at the same level of theory, are also listed. At equilibrium, the buckling parameter Δ varies in the range 0.51 – 0.85 Å. These values of the buckling parameter fall in the range of values obtained for other 2D sheets [41].

As expected, the lattice constant (a) and the buckling parameter (Δ), gradually increase with the atomic number/atomic size of the group-III element involved. The values vary from a = 3.89 Å (BBi) to a = 4.80 Å (InBi), and Δ = 0.51 Å (BBi) to Δ = 0.85 Å (InBi). Our results demonstrate that, in terms of structure, the LB sheets of BBi, AlBi, GaBi, and InBi are quite similar among them. This makes them compatible systems, from a point of view of hetero-structures, as well as possible layered materials and assemblies built upon different 2D templates [42]. For example, substrate such as MoS_2, h-BN are the most promising template for doing this [29, 30]

Table 1 also lists the cohesive energies per atom ($E_{coh/atom}$) of all hexagonal sheets of XBi. As expected, cohesive energies of the LB XBi sheets (3.25 – 2.15 eV) are lower than the ones calculated at the same level of theory for graphene (7.83 eV), and h-BN (7.12 eV). However, they are comparable to the cohesive energy of silicene (3.98 eV). As in the case of silicene, a possible way of assisting the synthesis of stable XBi sheets would be its growth upon an appropriate substrate [43-44].

In the following, we discuss the structural properties of the hexagonal sheets of XBi_3 (X = B, Al, Ga, and In). Due to their more complex eight-atom unit cells, the XBi_3 sheets are characterized by lattice parameters in the range of 8.17 - 9.12 Å (Table 1). The equilibrium structure for the case of $GaBi_3$ is displayed in figure 2(a). At equilibrium, the XBi_3 sheets can be structurally represented as two inter-penetrating sublattices, consisting of atoms X and Bi, respectively, and described by the respective buckling parameters Δ_1

and Δ_2, each one associated with the sublattices as shown in the bottom of figure 2(a). For these two buckling parameters, Δ_1 and Δ_2, a trend similar to the one discussed above for the sheets of XBi is also observed. However, the increase in their value with the atomic number/atomic size of the group-III element involved is less pronounced. Another finding in this computational study is that the sublattice corresponding to the group-III elements is significantly less buckled (Δ_1 = 0.48 – 0.69 Å) than the sublattice consisting of Bi atoms (Δ_2 = 1.84 – 1.88 Å), which apparently plays a role of a "framing" sublattice of the XBi_3 sheets. This behavior is similar to the one observed for the cases NSi_3 and PSi_3 [31-33].

The phonon spectra of all equilibrium structures of the XBi_3 systems were also calculated. Figure 2(b) displays the phonon spectrum of $GaBi_3$, as an example illustrating the absence of any negative frequencies of significant intensity. This confirms that all the XBi_3 sheets are dynamically stable. We emphasize that these findings are similar to those previously obtained for HB lead and tin layers [45].

Table 1 also lists the structural parameters, as well as the X-Bi and the Bi-Bi bond lengths, corresponding to the equilibrium structures of all XBi_3 sheets. In terms of buckling, the XBi_3 sheets exhibit a similar behavior (albeit more buckled) when compared to the buckling of the XBi sheets. Still, the fully relaxed structures of the BBi_3, $AlBi_3$, $GaBi_3$ and $InBi_3$ sheets remain of the LB type.

The cohesive energy calculated for the XBi_3 (Table 1) indicates that the sheets of BBi_3, $AlBi_3$ and $InBi_3$ exhibit similar energetic stability, albeit with a slightly higher $E_{coh/at}$, in comparison to the corresponding sheets of BBi, AlBi, and InBi. This is especially pronounced in the case of B and In. BBi and BBi_3 exhibit cohesive energies of 3.25 and 2.80 eV, respectively, whereas InBi and $InBi_3$ exhibit cohesive energies of 2.15 and 1.89 eV, respectively. On the other hand, when comparing the XBi_3 with XBi sheets containing the III-elements with intermediate atomic numbers, i. e., X = Al and Ga, we found that they exhibit much closer cohesive energies (see Table 1). The slightly less favorable energetic behavior of XBi_3, as compared to XBi (with exception of the GaBi), may be attributable to different bonding arrangements, due to the different composition of XBi_3 and XBi, as well as to the presence of homo-nuclear Bi-Bi bonds in XBi_3.

3.2. Electronic structure and topological properties of the XBi and XBi_3 sheets

The partial densities of states (PDOS) and corresponding band structures, calculated without spin-orbit coupling (SOC) and with SOC, for the equilibrium structures of all considered sheets of XBi and XBi_3 (X = B, Al, Ga, and In), are displayed

in figures 3 and 4, respectively. Quantitative differences among the systems arise from the contributions of the *p* states of Bi and X atoms to the PDOS near the Fermi level. Although these systems are structurally similar to silicene and germanene [40-46], the electronic structures are significantly different, leading to a tunable band gap opening, instead of forming gapless systems.

The corresponding band gaps, obtained without and with SOC, are listed in Table 1. As can be seen from figures 3(a)-(d), within the XBi class before including SOC in the calculations, the band structures of the distinct compounds appear qualitatively similar, exhibiting parabolic bands at the Γ point, although the band gap varies from 100 up to 750 meV. In fact, it is known that, when one employs the Heyd-Scuseria-Ernzerhof hybrid functional, these band gaps may significantly be increased but resulting in similar band structures [37, 48]. Additionally, these XBi systems exhibit direct band gaps, at the Γ point in the cases for Al to In and at the K point for B. Similarly, the Bi-containing topological insulators Bi_2Te_3 and Bi_2Te_2Se have recently been obtained as direct-gap semiconductors [48], when SOC is not taken into account. However, by including SOC, these materials exhibit dramatic changes in the band structures, indicating possible applicability connecting thermoelectric performance and topological insulating properties.

In the sense of investigating and classifying possible topological insulating characteristics of the XBi and XBi_3 sheets, we have also considered the inclusion of SOC into the electronic structure calculations. Chuang and collaborators [29] have previously observed topological properties only for the XBi family. We have analyzed the s-orbitals projection in the wave function in the band structures for all these systems. In the case of XBi sheets, the observed band inversion could be qualitatively employed to classify their topological-insulating nature. As a typical example of 2D topological insulator, we display in figure 5(a), we display the band structure of GaBi, without and with SOC, where it is demonstrated that the contribution of the s-orbitals moves from the bottom of the conduction band to higher energies. For the buckled equilibrium XBi structures, the band inversion was observed only in the GaBi and InBi hetero-sheets. On the other hand, a similar band inversion was not observed in the XBi_3 compounds, since there is no contribution of s-orbitals at the bottom of their respective conduction bands. In figure 5 (b), we illustrate the case of $GaBi_3$, although this behavior arises for all XBi_3 sheets. Further insight can be obtained from the band inversion strength, which is defined as the

direct band gap at the Γ point, being positive when the band is inverted and negative otherwise [29]. As displayed in figure 6, only GaBi and InBi present negative values for this quantity. We noticed that the same analysis can not be applied to the XBi_3 sheets since they do not present band inversion at the Γ point.

We have also noticed first that the band structures of XBi appear modified by spin-orbit effects and, especially, the band degeneracy is broken at the Γ point. Nonetheless, the calculated band structures with SOC continue to exhibit comparatively parabolic band edges. Now, we find the band gaps to be indirect and varying from 170 up to 480 meV. More interestingly, we have observed a small reduction (~6%) in the band gap of BBi and a strong reduction (~55%) in the band gap of AlBi. Conversely, we have observed a large increase (~37%) in the band gap of GaBi and a small increase (3%) in the band gap of InBi. We also emphasize that one of the effects of including SOC in the calculations is also lifting the spin degeneracy [49] of the calculated bands for the XBi systems, as shown in figure (3). Based on the electronic structure, the changes produced by SOC effects make the XBi sheets potential candidates to be exploited as topologically insulating 2D materials.

In turn, when the electronic properties of the XBi_3 sheets are calculated without considering SOC, most of them appear as narrow-band-gap semiconductors. For example, BBi_3, $AlBi_3$, and $GaBi_3$ exhibit very small band gaps of less than 80 meV, while the $InBi_3$ sheet opens a small band gap of 169 meV (see Table I and figure (4)). With the exception of BBi_3, the XBi_3 sheets exhibit band degeneracies at the Γ point with comparatively parabolic bands, as in the case of XBi. We also noticed that the XBi_3 sheets only exhibit an indirect band gaps in the cases of X = B, Al and Ga. By including SOC into the calculations, in general larger band gaps of the XBi_3 sheets are obtained; i.e., 526, 263, 286, and 244 meV for the BBi_3, $AlBi_3$, $GaBi_3$, and $InBi_3$, respectively. In addition, the inclusion of SOC removes the band degeneracies at the Γ point, with the exception of BBi, which as already pointed out, does not exhibit this degeneracy. This may be the reason for the enormous increase on the band gap in the case of BBi upon SOC inclusion. Another peculiarity of BBi is that it presents the higher value for the Δ_1 buckling parameter, breaking the planarity of the B-Bi bonds. The nature of the band gap, direct or indirect, is not affected by inclusion of SOC, with the exception of $AlBi_3$, which becomes now an indirect-gap semiconductor.

CONCLUSIONS

From first-principles calculations, the sheets of XBi and XBi_3 emerge as two classes of energetically and dynamically stable 2D materials, consisting of group-III elements and bismuth. Similarly to the case of other 2D sheets, the considered XBi (X = B, Al, Ga, In) sheets exhibit low-buckled equilibrium geometries, while the XBi_3 can be structurally represented as two interpenetrating sublattices, consisting of alternating X and Bi atoms. The dynamical stability, combined with the tunable electronic properties (by changing the X element involved) of the XBi and XBi_3 sheets, renders them as being prospective candidates for applications in room-temperature spintronic devices.

With respect to the electronic properties of these materials, the band structures are strongly affected by including SOC into the calculations. Without SOC, the band structures of the XBi and XBi_3 hetero-sheets are qualitatively similar, exhibiting bulk gaps in the 100–750 meV range for XBi and 5–170 meV range for XBi_3. The inclusion of SOC into the calculations keeps a similarity among the band structures by changing the X element, although it leads to a band degeneracy breaking at the Γ point for most of the considered cases, and a large band gap opening for the XBi_3 sheets.

In all the cases of XBi, SOC changes the band gaps from direct to indirect, varying from 170 up to 480 meV, with a small reduction in the case of BBi and a strong one in the case of AlBi. Nonetheless, there is a large increase in the band gaps of GaBi and a small one in the case of InBi. Additionally, SOC causes the lifting in the spin degeneracy of the calculated bands for the XBi sheets. The band inversion calculated for the GaBi and InBi sheets indicates that they naturally represent 2D topological insulating phases. Since DFT is known to underestimate calculated band gaps, we stress that GaBi and InBi exhibit sizable gaps, in a range of 170–175 meV; i. e., sufficiently large for practical applications at room temperature.

For XBi_3, our calculations without SOC show that most of them are small gap semiconductors. Inclusion of SOC into the calculations causes significant band gap openings to a range of 240 to 530 meV in these systems. In this case there is no band inversion as observed in the XBi compounds, since there is no contribution of s-orbitals at the bottom of their conduction bands. However, it is hoped that unusual properties can emerge from these structures, e.g., in electron transport applications in low dimensions, mainly due to the increase of electronic states near the conduction band.

ACKNOWLEDGMENTS

The authors gratefully acknowledge partial financial support for this work by the Swedish Research Council (VR) through Swedish Research links project 348-2014-4249. G.K.G. and A. K. G. gratefully acknowledge support by the Linköping Linnaeus Initiative for Novel Functionalized Materials (LiLi-NFM, VR). G. K. G. acknowledges support by the Swedish Foundation for Strategic Research (SSF) Synergy Grant #RMA11-0029 on Functional Carbides and Advanced Surface Engineering (FUNCASE). R.R., C.M.C.deC., and F.deB.M. acknowledge ConselhoNacional de DesenvolvimentoCientífico e Tecnológico (CNPq) and Fundação de Amparo à Pesquisa do Estado da Bahia (FAPESB) for partial support. R.R.Q.F. acknowledges the support by Coordenação de Aperfeiçoamento de Pessoal de Nível Superior (CAPES). We acknowledge the fruitful discussions with Dr. S. Cunha during the early stages of this work.

References

[1] Zhang S *et al* 2015 *Angew. Chem. Int.* **54** 1

[2] Rasche B *et al* 2013 *Nature Mater.* **12** 422

[3] Li Z*et al* 2015 *Nature Comm.* **6** 6321

[4] Zhang S *et al* 2015 *Proc. Natl. Acad. Sci. USA* 112 2372

[5] Balendhran S *et al* 2015 *Small* **11** 640

[6] Azevedo S *et al* 2009 *Eur. Phys. J. B* **67** 507

[7] Pakdel A, Bando Y and Golberg D 2014 *Chem. Soc. Rev.* **43** 934

[8] Fazzio A *et al* 2012 *J. Phys. Condens. Matter.* **24** 075301

[9] de Almeida Junior E F *et al* 2012 *Eur. Phys. J.B* **85**, 48

[10] Tsipas P *et al* 2013*Appl. Phys. Lett.***103** 251605

[11] S. Valedbagi S, Fathalian A and Elahi S M 2013 *Opt. Comm.* **309** 153

[12] Le M-Q 2014 *J. Comput. Theor. Nanoscience* **11** 1458

[13] Li H *et al* 2010 *J. Phys. Chem. C* 114 11390

[14] Liu H *et al* 2014 *ACS Nano* 8 4033

[15] Zhen Z and Tománek D 2014 *Phys. Rev. Lett.* 112 176802

[16] "The Nobel Prize in Physics 2014 - Advanced Information" 2015 Nobelprize.org. Nobel Media AB
<http://www.nobelprize.org/nobel_prizes/physics/laureates/2014/advanced.html>

[17] Janotti A, Wei S-H and Zhang S B 2002 *Phys. Rev. B* **65** 115203

[18] Ferhat M and Zaoui A 2006 *Appl. Phys. Letters* **88** 161902

[19] Ferhat M and A. Zaoui 2006 *Phys. Rev. B* **73**, 115107

[20] Keen B *et al* 2014 *Journal of Electronic Materials* **43** 914

[21] La Fontaine A and Keast V J 2006 *Mater. Charact.* **57** 424

[22] Witkin D 2012 *J. Electron. Mater.* **41** 190

[23] Uenishi K, Hayong K and Kobayashi K F1996 *J. Mater. Sci.* **31** 3605

[24] Kaban I G and Hoyer W 2008 *Phys. Rev. B* **77** 125426

[25] Waters J *et al* 2003 *J. Mater. Sci.: Mater. Electro.* **14** 599

[26] Vehkamäki M T *et al* 2006 *Chem. Mater.* **18** 3883

[27] Zhou J-J *et al* 2014 *Nano Lett.***14** 4767

[28] Zhu Z-H *et al* 2014 Phys. Rev. Lett. 112 076802

[29] Chuang F-C *et al* 2014 *Nano Lett.***14** 2505

[30] Huang Z-Q *et al* 2013 *Phys. Rev. B* **88** 165301

[31] Ding Y and Wang Y 2013 *J. Phys. Chem. C* **117**, 18266

[32] Luo X *et al* 2011 *J. Am. Chem. Soc.* **133** 16285

[33] Ding Y and Wang Y 2014 *J. Phys. Chem. C* **118** 4509

[34] Kresse G and J. Hafner 1993 *Phys. Rev. B* **47** 558; Kresse G and Furthmüller 1996 *Phys. Rev. B*1996 **54** 11169

[35] Perdew J P. K. Burke and Ernzerhof M 1996 *Phys. Rev. Lett.* **77** 3865

[36] Kresse G and Joubert D 1999 *Phys. Rev. B* **59** 1758

[37] Ma Y *et al* 2015 *Phys. Rev. B* **91** 235306

[38] Hobbs D et al 2000 *Phys. Rev. B* **62** 1156

[39] Togo A, Oba F and Tanaka I 2008 *Phys. Rev. B* **78** 134106

[40] Cahangirov S *et al* 2009 *Phys. Rev. Lett.***102**, 236804

[41] Sahin H *et al* 2009 *Phys. Rev. B* **80** 155453

[42] Gao G *et al* 2012*Nano Lett.***12** 3518

[43] Lalmi B *et al* 2010 *Appl. Phys. Lett.* **97** 223109 and 2010 *Phys. Lett.* **97** 223109

[44] Fleurence A *et al* 2012 *Phys. Rev. Lett.* **108** 245501

[45] Rivero P *et al* 2014 *Phys. Rev. B* **90** 241408(R)

[46] Pan Y *et al* 2014 Small **10** 2215

[47] Peralta J E *et al* 2006 *Phys. Rev. B* **74** 073101

[48] Shi H *et al* 2015 *Phys. Rev. Appl.* **3** 014004

[49] Ma D, Li Z and Yang Z 2012 Carbon **50** 297

Tables

TABLE I. Calculated structural parameters (in Å), cohesive energies per atom (in eV), and energy gaps (in meV) for the XBi and XBi_3 (X = B, Al, Ga, In) relaxed sheets. Results for graphene, silicene and h-BN are provided at the same level of calculations for comparison.

2D system	Buckling Type	a	Δ or Δ_1; Δ_2	d_{Bi-X}	d_{Bi-Bi}	$E_{coh/at}$	E_g	E_{g-SOC}
graphene	planar	2.46	-	-	-	7.83	-	-
silicene	LB	3.87	0.45	-	-	3.98	-	-
h-BN	planar	2.51	-	-	-	7.12	4 680[b]	-
BBi	LB	3.89	0.51	2.30	-	3.25	511[b]	479[c]
		3.891[a]	0.51[a]					
AlBi	LB	4.53	0.77	2.73	-	2.56	751[b]	335[c]
		4.523[a]						
GaBi	LB	4.52	0.79	2.73	-	2.31	107[b]	169[c]
		4.521[a]						
InBi	LB	4.80	0.85	2.90	-	2.15	169[b]	175[c]
		4.805[a]	0.85[a]					
BBi_3	buckled	8.17	0.69; 1.84	2.33	3.06	2.80	5[c]	526[c]
$AlBi_3$	buckled	8.83	0.48; 1.85	2.77	3.04	2.45	80[c]	263[b]
$GaBi_3$	buckled	8.82	0.56; 1.86	2.77	3.03	2.33	81[c]	286[c]
$InBi_3$	buckled	9.12	0.58; 1.88	2.96	3.03	1.89	169[b]	244[b]

[a] Results as obtained in Ref. [26]

[b] Direct band gap

[c] Indirect band gap

Figures

Figure 1. (a)Top and side views of the LB equilibrium structure of the GaBi sheet (Δ = 0.79 Å);(b) Variation of the total energy with respect to the lattice constant for the XBi(X = B, Al, Ga, In) sheets; (c) Phonon spectra corresponding to the LB GaBi sheet; and(d) Phonon spectra for the HB GaBi sheet.

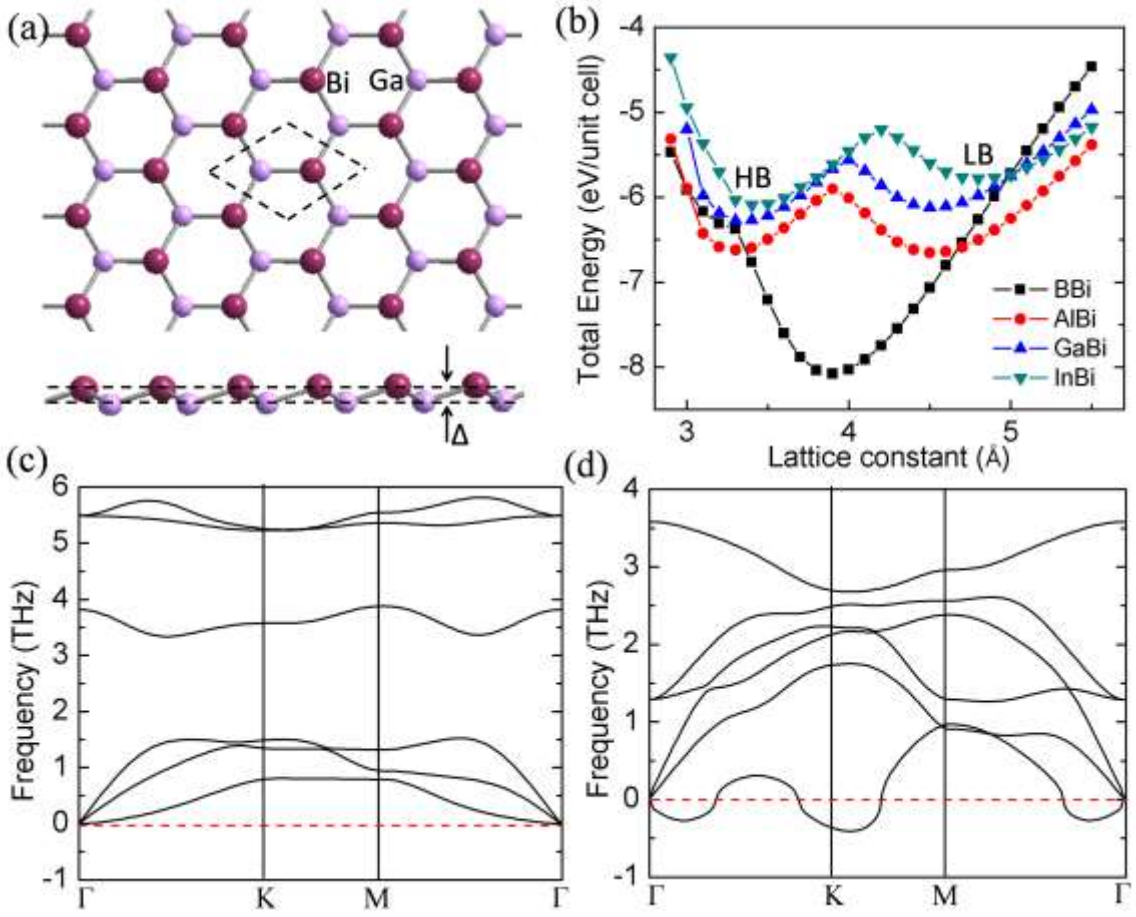

Figure 2. (a) Top and side views of the equilibrium structure of the $GaBi_3$ sheet (Δ_1 = 0.56 Å, Δ_2 = 1.86 Å); (b) Phonon spectra corresponding to the$GaBi_3$ sheet. Fermi level was set to zero energy.

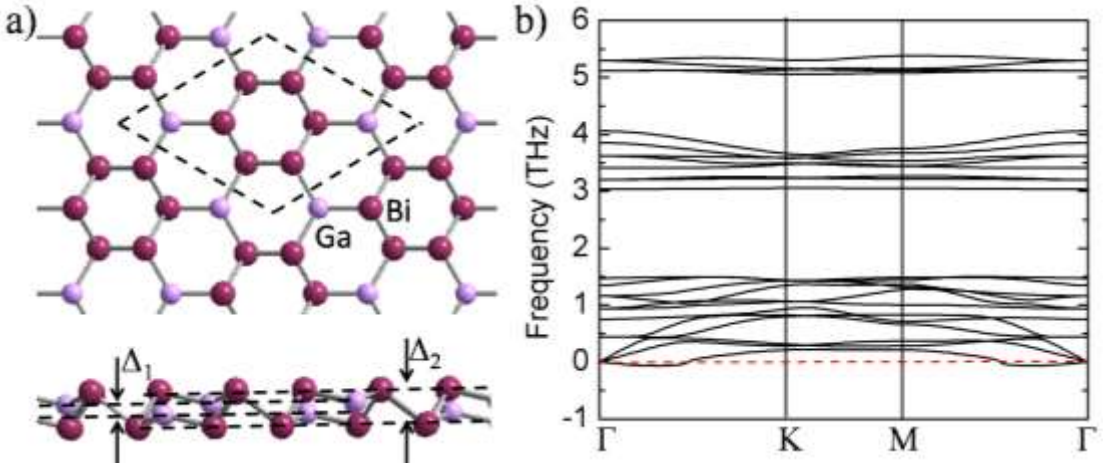

Figure 3. Partial densities of states and band structures obtained without spin-orbit coupling (SO), and with SO for the XBi sheets: (a) BBi, (b) AlBi, (c) GaBi, and (d) InBi. Fermi level was set to zero energy.

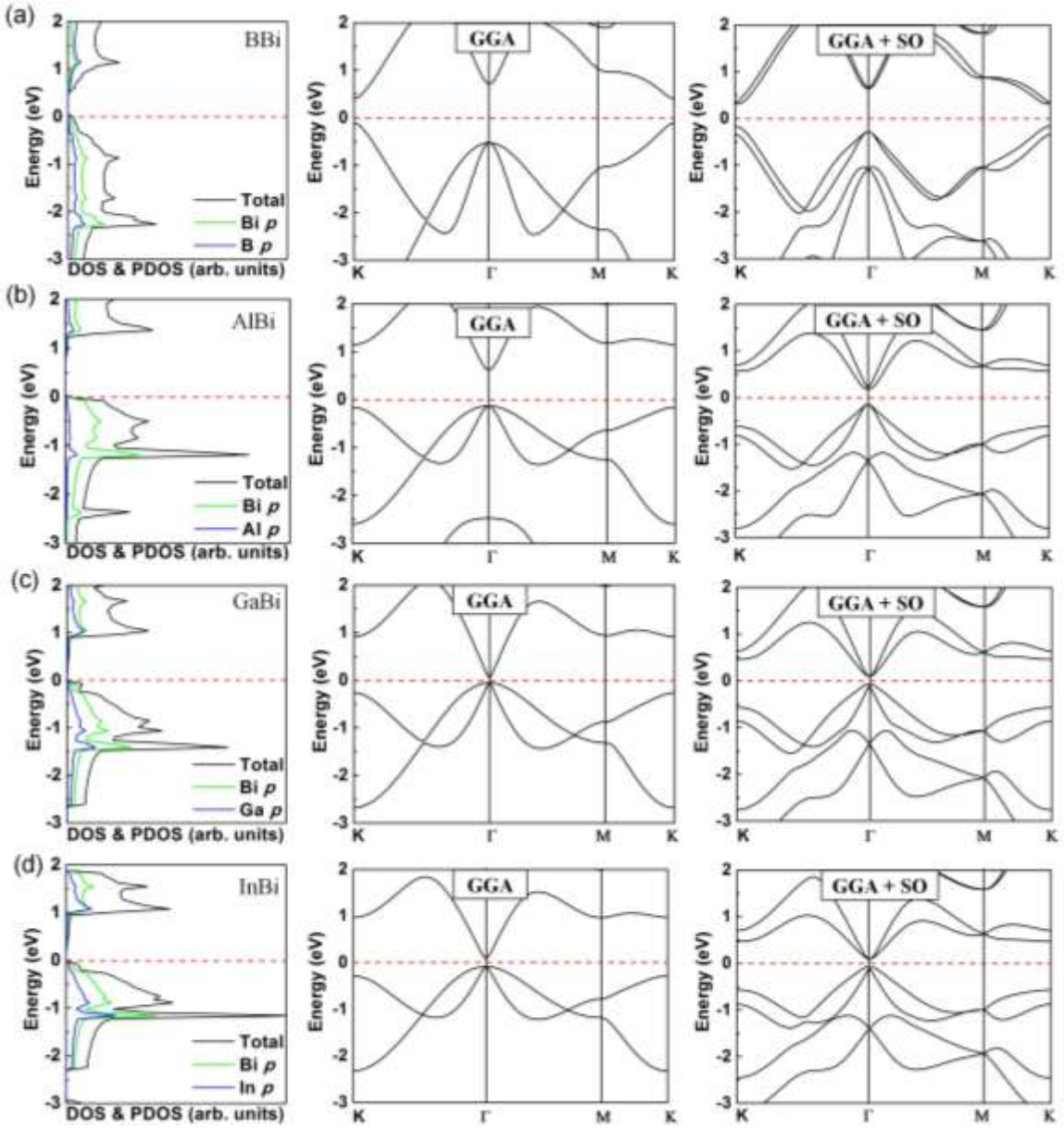

Figure 4. Partial densities of states and band structures obtained without SO and with SO for the XBi_3 sheets: (a) BBi_3, (b) $AlBi_3$, (c) $GaBi_3$, and (d) $InBi_3$. Fermi level was set to zero energy.

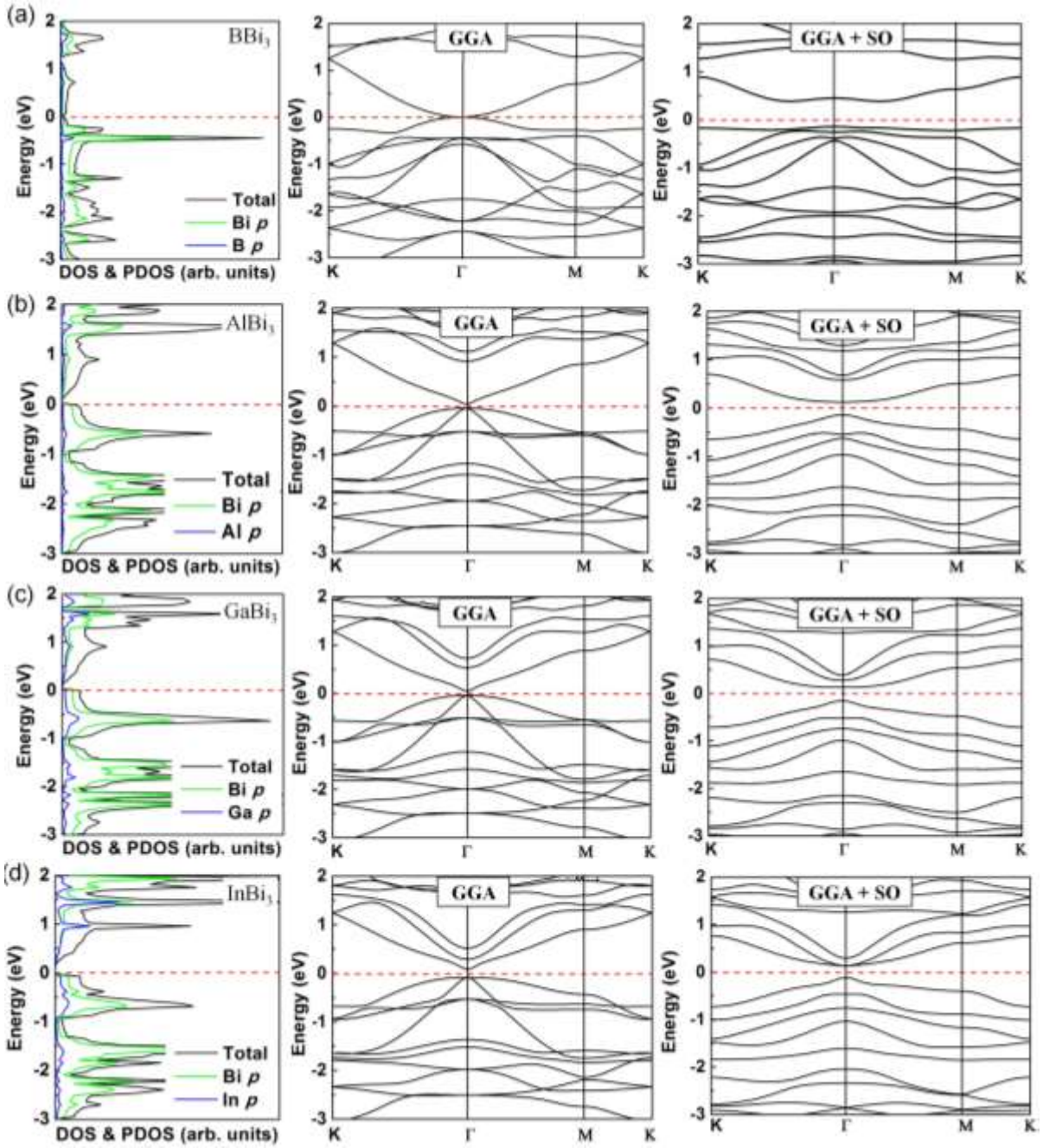

Figure 5. Band structure without and with SO coupling for (a) GaBi and (b) $GaBi_3$. The size of the red circles is proportional to the contributions of the s-orbitals to the wave functions.

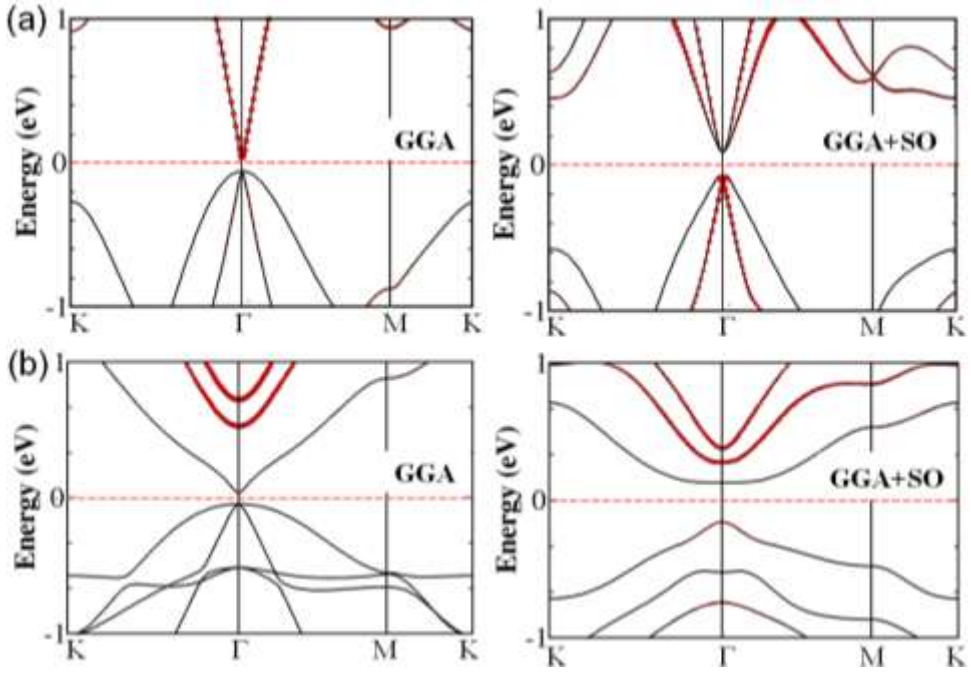

Figure 6. Band inversion strength at the Γ point for the XBi sheets.